applied optics

High-performance visible blind ultraviolet photodetector based on $KTaO_3$ single crystal

Jing-ting Yang,[1] Chen Ge,[1,*] Kui-juan Jin,[1,2,3] Hui-bin Lu,[1] and Guo-zhen Yang[1,2]

[1]Institute of Physics, Chinese Academy of Sciences, Beijing 100190, China
[2]Collaborative Innovation Center of Quantum Matter, Beijing 100190, China
[3]e-mail: kjjin@iphy.ac.cn
*Corresponding author: gechen@iphy.ac.cn

Received 14 December 2015; revised 3 February 2016; accepted 4 February 2016; posted 4 February 2016 (Doc. ID 255751); published 16 March 2016

We report a visible-blind ultraviolet photoconductive detector with interdigitated electrodes based on $KTaO_3$ (KTO) single crystals. Both the steady spectral responses and the transient photovoltaic measurements clearly exhibit a cutoff wavelength at 344 nm (~3.6 eV), in accordance with the bandgap of KTO. The KTO photodetectors show a low dark current ~1.5 pA at 20 V, and a high UV-to-visible rejection ratio with 3 orders of magnitude at room temperature. The quantum efficiency is 37.49% under 20 V bias, and the detectivity D^* of 3.85×10^{12} cm · $Hz^{0.5}$/W, which is comparable to that of silicon photodetectors in the UV region. The rise time of photoelectric response is ~260 ps, indicating an ultrafast photoelectric response characteristic. The present work offers appealing prospects for the application of KTO materials in high-performance visible blind ultraviolet photodetectors.

OCIS codes: (040.0040) Detectors; (040.7190) Ultraviolet; (040.5160) Photodetectors.

http://dx.doi.org/10.1364/AO.55.002259

1. INTRODUCTION

Ultraviolet (UV) photodetectors have drawn a great deal of interest for their broad applications such as flame safeguard, fire control, missile tracking and intercept, and environmental monitoring [1]. Conventional semiconductor silicon with a narrow bandgap is not an ideal material for UV photodetectors because it needs filters to block visible light. The materials with a wide bandgap, such as diamond [2], III–V nitrides [3,4], silicon carbide [5], and zinc oxide [6], have attracted much attention in UV photodetectors. However, these photodetectors mostly require a complex and expensive fabrication process. Perovskite oxides with wide bandgaps have great potential to be the next-generation UV photodetectors. In the past few years, much attention has been paid to the photodetectors based on perovskite oxides, including $SrTiO_3$ [7,8], $LaAlO_3$ [9], $LiTaO_3$ [10], $LaSrAlO_4$ [11], and $LiNbO_3$ [12]. $KTaO_3$ (KTO), as a cubic perovskite oxide, display quantum paraelectricity [13], and high mobility n-type conduction with doping [14]. It is worth mentioning that the ultrafast photovoltaic response in tilted KTO single crystals has been recently investigated. The rise time and FWHM are 497.4 ps and 974.6 ps, respectively [15]. With a large bandgap of 3.5–3.75 eV [16–19] and the potential ultrafast response ability for the ultraviolet light, we anticipate that it has a unique potential application in photodetectors. In the present work, we report for the first time, to the best of our knowledge, a visible-blind UV photodetector based on KTO single crystals. This photodetector shows a low dark current of ~1.5 pA, a high UV-to-visible rejection ratio with 3 orders of magnitude at room temperature, a responsivity of ~100 mA/W, a rise time of ~260 ps, and a good detectivity D^* of 3.85×10^{12} cm · $Hz^{0.5}$/W at 20 V under light illumination with a wavelength of 316 nm, which could be one of the promising candidates as the novel UV photodetectors.

2. EXPERIMENTAL DETAILS

We used commercial KTO (001) single crystal (MTI Corporation). The size of KTO wafer is 10 mm × 10 mm with a thickness of 0.5 mm. Employing the standard photolithography and thermal evaporation techniques, we fabricated interdigitated Au electrodes with a thickness of 75 nanometers on KTO. The optical images of devices with various finger widths are shown in Fig. 1. The finger width (w) of the electrodes is equal to the separated spacing (s). In this work, we fabricated photodetectors with various w of 10 [Fig. 1(a)], 20 [Fig. 1(b)], and 30 μm [Fig. 1(c)], in order to investigate the photoresponse dependence on the finger width of interdigitated electrodes.

A 150 W Xeon lamp (Zolix Corporation) was utilized as the light source. Combined with a monochromator, it can export

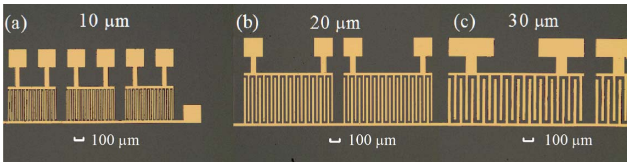

Fig. 1. Optical images of the interdigitated electrodes with finger widths of 10 (a), 20 (b), and 30 μm (c) on KTO.

continuous light with wavelengths from 200 to 1100 nm. The light intensity was calibrated by a power meter (Ophir Nova II), and the current was measured by a semiconductor parameter analyzer (Agilent B1500A). A 500 MHz oscilloscope (Tektronix TDS3052B) was used for measuring the steady-state and transient photoelectric signals. A 2.5-GHz oscilloscope (Tektronix TDS7254B) was also used for measuring ultrafast photoelectric response. We used a picosecond laser with a wide tunable optical parameter (EKSPLA PL2210A/PG403-SH/PG703-DFG) as the light source in the measurement of transient photoelectric response. The output wavelength of the laser can be tuned from 230 nm to 16 μm, and the pulse duration is 25 ps.

3. RESULTS AND DISCUSSION

The KTO photodetector with a finger width of 30 μm is studied, as shown in Fig. 2. Figure 2(a) is the spectral response of KTO photodetector at 1 V (red), 2 V (blue), and 5 V (green) bias. The responsivity turned to be larger with the increasing voltage. All the results performed under various voltages exhibit a cutoff wavelength of this photodetector locating at 344 nm (~3.61 eV), which is consistent with the absorption edge of KTO, as shown in Fig. 2(b). The cutoff wavelength and the absorption edge indicate KTO with a bandgap ~3.6 eV, which agrees well with the reported values 3.5–3.75 eV of KTO crystal [16–19]. The responsivity increases with decreasing the light wavelength and does not show saturation until a wavelength of 300 nm. Here, we define UV-to-visible rejection ratio as the responsivity measured at 316 nm divided by the responsivity measured at 400 nm. With such a definition, we achieve a UV-to-visible rejection ratio of ~2300 at 5 V. And the ratio of photocurrent at 316 nm to dark current is extremely high, with 4 orders of magnitude at room temperature. The mechanism of photocurrent of KTO detectors with interdigitated electrodes can be easily understood as the following way. Photoinduced carriers can be generated in the KTO crystal, when the photon energy is higher than the bandgap of KTO. Then, these photoinduced carriers can migrate toward the electrodes under an external bias to form an electrical current. Figure 2(c) shows the dependence of the photocurrent on the power density of the light illumination with a wavelength of 316 nm. Clearly, the photocurrent of the detector with a finger width of 30 μm increases linearly with the power density according to our fitting results. Figure 2(d) shows the dependence of the photocurrent on the bias voltage under light illumination with a wavelength of 316 nm with different optical power densities. The photocurrent increases with bias under light illumination with all optical power densities. At the same bias,

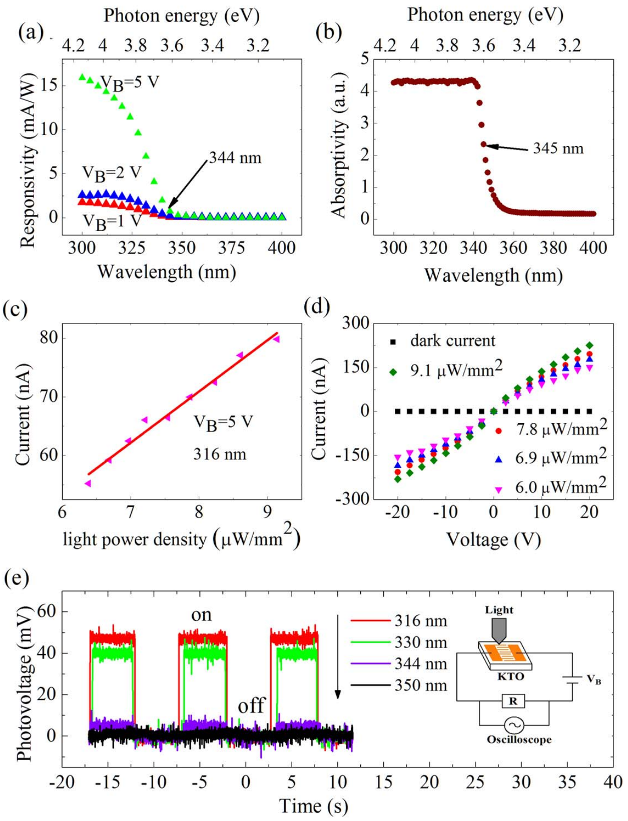

Fig. 2. (a) Spectral response of the KTO photodetector with a finger width of 30 μm at 1 V (red), 2 V (blue), and 5 V (green) bias. (b) Absorption spectra of $KTaO_3$ single crystal. (c) Photocurrent variation with the optical power density under illumination of 316 nm UV light at 5 V bias. (d) Photocurrent dependence of the bias voltage under light illumination with a wavelength of 316 nm with different optical power densities. (e) Steady-state photoelectric response of one interdigitated electrode cell with a 30 μm finger width on $KTaO_3$ detector under light illumination of different wavelengths at 5 V bias. Inset shows the schematic of measurement circuit for the steady-state measurement.

the photocurrent increases with increasing optical power density. Figure 2(e) is the steady-state photovoltage of KTO photodetector under light illumination with wavelengths of 350, 344, 330, and 316 nm. And the inset image is the schematic of measurement circuit. The KTO photodetector is in series with a tunable DC voltage source V_b, and a sampling resistance R of 1 MΩ. A 500 MHz digital oscilloscope was used for measuring the voltage of sampling resistance R. No photovoltage signals are observed when the photon energy is smaller than the bandgap (black curve). The photovoltage is high because of induced photocurrent in the circuit, when the Xe lamp with wavelength of 316, 330, or 344 nm is switched on. The photovoltage increases with the wavelength from 344 to 316 nm, corresponding to the responsivity of Fig. 2(a). Under illumination with a wavelength of 316 nm, the output voltage of oscilloscope is 47.17 mV, and the corresponding photocurrent induced in the circuit is 47.17 nA.

In order to investigate the transient photoelectric response process, we used a 500 MHz digital oscilloscope to carry out

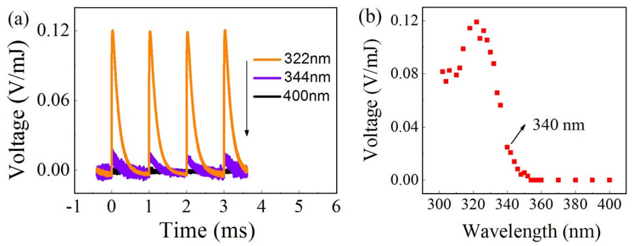

Fig. 3. (a) Transient photovoltage of KTO detector with a finger width of 30 μm, measured by a 500 MHz oscilloscope at 1 V bias. (b) Peak of transient photovoltage as a function of the wavelength of laser.

the photovoltage measurements under the pulsed laser with various wavelengths. Figure 3 is the transient photovoltage of the KTO detector as a function of pulsed laser wavelength with a finger width of 30 μm. All the measured photovoltage with various wavelengths were divided by the corresponding laser pulse energy. As shown in Fig. 3(a), no photovoltage signals are observed when the photon energy is smaller than the bandgap (black curve). The photovoltage under pulsed laser illumination with a wavelength of 322 nm is larger than that of 344 nm, as shown in Fig. 3(a). The decay times of 344 and 322 nm laser are 0.22 and 0.16 ms, respectively. Figure 3(b) represents the peak of transient photovoltage as a function of laser wavelength. The cutoff wavelength of Fig. 3(b) is consistent with that of spectral responsivity in Fig. 2(a). Furthermore, we characterized the fast photoelectric response behavior of the KTO detectors by using a 2.5 GHz oscilloscope, as shown in Fig. 4. The pulse duration and wavelength of the pulsed laser are 25 ps and 316 nm, respectively. The rising edge (10%–90%) and FWHM are ~260 ps and ~1 ns, respectively, indicating an ultrafast response in our KTO photodetectors.

The responsivity dependence on the finger width of interdigitated electrodes was studied under continuous light illumination with a wavelength of 316 nm. Figures 5(a)–5(c) represent the photocurrent and dark current of the devices with finger widths of 10, 20, and 30 μm, respectively. All the devices with various finger widths exhibit a rather low dark current ~1.5 pA under 20 V bias. The photocurrent, under illumination with a wavelength of 316 nm, increases with increasing bias. From Fig. 1, we can see the active areas (the areas directly exposed to radiation) are 0.084, 0.235, and 0.357 mm^2 for detectors with finger widths of 10, 20, and 30 μm, respectively. Although the photocurrent of detector with a finger width of 10 μm is smaller than that of the other, but its responsivity is the largest due to the minimum illumination area. Figure 5(d) shows that the photocurrent responsivity and corresponding quantum efficiency at 20 V bias are decreasing with the increasing finger width of interdigitated electrodes. The photocurrent dependence on finger width and bias voltage described above is owing to the carriers' transit time τ_t, which is proportional to finger width (or the interspace of two fingers) and inversely proportional to the bias voltage.

In order to obtain a strong sensitivity, the photocurrent signal needs to be maximized. The quantum efficiency η describes how well the detector is coupled to the radiation to be detected. It is defined as the number of carriers generated by each photon or [20]

$$\eta = R_i hc/\lambda q, \tag{1}$$

where R_i is the spectral current responsivity, λ is the wavelength, h is Planck's constant, c is the light velocity, and q is the electron charge. According to Eq. (1), in Fig. 5(d), the quantum efficiency decreasing with increasing finger widths is owing to the decreasing responsivity. The value of the quantum efficiency for photon energies above the bandgap depends on the finger width, the material quality, and the bias. The quantum efficiency can obtain 37.49% with finger width of 10 μm at 20 V, which is higher than many detectors based on single crystals, such as ZrO_2 [21], $LiTaO_3$ [10], and $LiNbO_3$ [12].

Detectivity D^* is the main parameter characterizing normalized signal-to-noise performance of detectors and can be defined as [1,22]

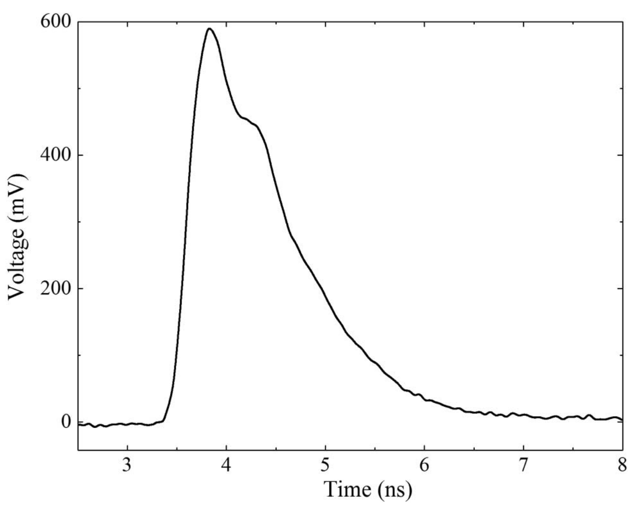

Fig. 4. Ultrafast photoelectric response of KTO detector with a finger width of 30 μm at 5 V bias, measured by a 2.5 GHz oscilloscope, and a laser with pulse width of 25 ps.

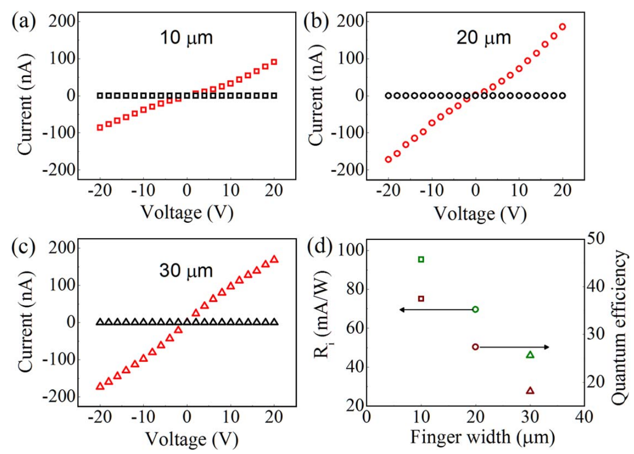

Fig. 5. (a)–(c) I–V characteristics of detectors with three different interdigital electrodes in dark (black symbols) or in light illumination with a wavelength of 316 nm (red symbols). (d) Finger width dependence on photocurrent responsivity and corresponding quantum efficiency at 20 V.

$$D^* = R_i(A\Delta f)^{1/2}/I_n, \quad (2)$$

where A is the active area of detector, Δf is the frequency band, R_i is the current responsivity, and I_n is the current noise due to generation and recombination processes. There are three contributions to the noise that limit D^*: shot noise from dark current, Johnson noise, and thermal fluctuation "flicker" noise. Here, the thermally limited mode may not be applied as the shot noise is significant. Therefore, the noise current source can be evaluated by [8,22]

$$I_n = [(4k_B T/R_{\text{dark}} + 2qI_{\text{dark}})\Delta f]^{1/2}, \quad (3)$$

where R_{dark} is the differential resistance at the bias point, I_{dark} is the dark current at the bias point, T is the temperature, K_B is the Boltzmann constant, and q is the electron charge. According to Eqs. (2), (3), we can calculate the D^*. With a 20 V applied bias at 316 nm, the corresponding D^* of detector with finger widths of 10, 20, and 30 μm are $3.85 \times 10^{12}\ \text{cm} \cdot \text{Hz}^{0.5}/\text{W}$, $5.60 \times 10^{12}\ \text{cm} \cdot \text{Hz}^{0.5}/\text{W}$ and $3.09 \times 10^{12}\ \text{cm} \cdot \text{Hz}^{0.5}/\text{W}$, respectively. From the data of Fig. 2(a), we can calculate that the η and D^* of detector with a finger width of 30 μm are 6.58% and $4.02 \times 10^{12}\ \text{cm} \cdot \text{Hz}^{0.5}/\text{W}$ at 5 V bias, respectively, under light illumination with a wavelength of 300 nm. In the UV region, the D^* of Si-based is in the magnitude of $10^{12}\ \text{cm} \cdot \text{Hz}^{0.5}/\text{W}$ [8]. It means that the D^* of our detectors can be comparable with Si-based photodetectors in UV detection. Si photodetectors require bulky band filters to block the visible solar radiation [1]. But our devices are free from the mentioned shortcoming for its intrinsic wide bandgap. Moreover, the small dark current with about 1.5 pA, good signal-to-noise ratio (D^*), and the rise time of ~260 ps show its feasibility for applying in low noise and ultrafast UV detectors. Therefore, it is expected that KTO detectors with a simple fabrication process have unique potential in UV detection applications.

4. CONCLUSION

We fabricated the photodetectors based on $KTaO_3$ single crystal with an interdigitated electrode of different finger widths. A wavelength cutoff was experimentally observed at 344 nm, corresponding to the bandgap 3.6 eV of KTO. The photodetector shows a low dark current of ~1.5 pA, quantum efficiency of 37.49%, an ultrafast rise time of ~260 ps, a high UV-to-visible rejection ratio with 3 orders of magnitude at room temperature, and detectivity D^* of $3.85 \times 10^{12}\ \text{cm} \cdot \text{Hz}^{0.5}/\text{W}$ under the light illumination with a wavelength of 316 nm. The detectivity D^*, $3.85 \times 10^{12}\ \text{cm} \cdot \text{Hz}^{0.5}/\text{W}$, of our detectors can be comparable with that of Si photodetectors in the UV detection range. Because of good device performance and simple fabrication process, it is expected that $KTaO_3$ could be one of the promising candidates in the next generation of novel UV photodetectors.

Funding. National High Technology Research and Development Program of China (2014AA032607); National Basic Research Program of China (2013CB328706); National Natural Science Foundation of China (NSFC) (11134012, 11404380, 11474349); Strategic Priority Research Program (B), Chinese Academy of Sciences (CAS) (XDB07030200).

Acknowledgment. We thank Prof. X. L. Xu for the help of photolithography.

REFERENCES

1. M. Razeghi and A. Rogalski, "Semiconductor ultraviolet detectors," J. Appl. Phys. **79**, 7433–7473 (1996).
2. Y. Koide, M. Liao, and J. Alvarez, "Thermally stable solar-blind diamond UV photodetector," Diam. Relat. Mater. **15**, 1962–1966 (2006).
3. Y. Zhang, S. C. Shen, H. J. Kim, S. Choi, J. H. Ryou, R. D. Dupuis, and B. Narayan, "Low noise GaN ultraviolet p-i-n photodiodes on GaN substrates," Appl. Phys. Lett. **94**, 221109 (2009).
4. C. J. Collins, T. Li, A. L. Beck, R. D. Dupuis, J. C. Campbell, J. C. Carrano, M. J. Schurman, and I. A. Ferguson, "Improved device performance using a semi-transparent p-contact AlGaN/GaN heterojunction positive-intrinsic-negative photodiode," Appl. Phys. Lett. **75**, 2138–2140 (1999).
5. A. Sciuto, F. Roccaforte, S. D. Franco, V. Raineri, and G. Bonanno, "High responsivity 4H-SiC schottky UV photodiodes based on the pinchoff surface effect," Appl. Phys. Lett. **89**, 081111 (2006).
6. C. Soci, A. Zhang, B. Xiang, S. A. Dayeh, D. P. R. Aplin, J. Park, X. Y. Bao, Y. H. Lo, and D. Wang, "ZnO nanowire UV photodetectors with high internal gain," Nano. Lett. **7**, 1003–1009 (2007).
7. L. Wang, K. J. Jin, J. Xing, C. Ge, H. B. Lu, W. J. Zhou, and G. Z. Yang, "High-sensitivity $SrTiO_3$ photodetectors with paralleled multiple interdigital electrode cells," Appl. Opt. **52**, 3473–3476 (2013).
8. W. J. Zhou, K. J. Jin, H. Z. Guo, C. Ge, M. He, and H. B. Lu, "Electrode effect on high-detectivity ultraviolet photodetectors based on perovskite oxides," J. Appl. Phys. **114**, 224503 (2013).
9. J. Xing, E. J. Guo, K. J. Jin, H. B. Lu, J. Wen, and G. Z. Yang, "Solar-blind deep-ultraviolet photodetectors based on an $LaAlO_3$ single crystal," Opt. Lett. **34**, 1675–1677 (2009).
10. E. J. Guo, J. Xing, H. B. Lu, K. J. Jin, J. Wen, and G. Z. Yang, "Ultraviolet fast-response photoelectric effects in $LiTaO_3$ single crystal," J. Phys. D **43**, 015402 (2010).
11. H. Ni, S. Q. Zhao, and K. Zhao, "Thickness-dependent photoresponse characteristics of miscut $LaSrAlO_4$ single crystals for ultraviolet detection," Appl. Opt. **49**, 2635–2638 (2010).
12. E. J. Guo, J. Xing, K. J. Jin, H. B. Lu, J. Wen, and G. Z. Yang, "Photoelectric effects of ultraviolet fast response and high sensitivity in $LiNbO_3$ single crystal," J. Appl. Phys. **106**, 023114 (2009).
13. K. A. Müller and H. Burkard, "$SrTiO_3$: an intrinsic quantum paraelectric below 4 K," Phys. Rev. B **19**, 3593–3602 (1979).
14. S. H. Wemple, "Some transport properties of oxygen-deficient single crystal potassium tantalite ($KTaO_3$)," Phys. Rev. **137**, A1575–A1582 (1965).
15. J. Xing, E. J. Guo, K. J. Jin, H. B. Lu, M. He, J. Wen, and F. Yang, "Ultraviolet sensitive ultrafast photovoltaic effect in tilted $KTaO_3$ single crystals," Chin. Phys. Lett. **27**, 027202 (2010).
16. S. H. Wemple, D. Kahng, and H. J. Braun, "Surface barrier diodes on semiconducting $KTaO_3$," J. Appl. Phys. **38**, 353–359 (1967).
17. E. Yamaichi, K. Watanabe, and K. Ohi, "The photoluminescence decay of the 2.2 eV-emission band in $KTaO_3$ single crystal," J. Phys. Soc. Jpn. **57**, 2201–2206 (1988).
18. G. E. Jellison, Jr., I. Paulauskas, L. A. Boatner, and D. J. Singh, "Optical functions of $KTaO_3$ as determined by spectroscopic ellipsometry and comparison with band structure calculations," Phys. Rev. B **74**, 155130 (2006).
19. S. Nazir, N. Singh, and U. Schwingenschlögl, "Charge transfer mechanism for the formation of metallic states at the $KTaO_3/SrTiO_3$ interface," Phys. Rev. B **83**, 113107 (2011).
20. S. M. Sze and K. K. Ng, *Physics of Semiconductor Devices* (Wiley, 2006).
21. J. Xing, E. J. Guo, and H. B. Lu, "High sensitive and ultrafast UV photodetector based on ZrO_2 single crystals," Sci. China Phys. Mech. Astron. **54**, 1416–1419 (2011).
22. K. W. Liu, J. Y. Zhang, J. G. Ma, D. Y. Jiang, Y. M. Lu, B. Yao, B. H. Li, D. X. Zhao, Z. Z. Zhang, and D. Z. Shen, "$Zn_{0.8}Mg_{0.2}O$-based metal-semiconductor–metal photodiodes on quartz for visible-blind ultraviolet detection," J. Phys. D **40**, 2765–2768 (2007).